Nitrogen fixation by an arc plasma at elevated pressure to increase the energy efficiency and production rate of NO$_x$

Ivan Tsonev‡, Colin O'Modhrain‡, Annemie Bogaerts, Yury Gorbanev*

Research group PLASMANT, Department of Chemistry, University of Antwerp, Universiteitsplein 1, 2610 Wilrijk, Belgium

‡These authors contributed equally. *Corresponding author. Phone: +32(0)32652343. E-mail: yury.gorbanev@uantwerpen.be.

Supporting Information

Pages: 25
Figures: 15
Tables: 4

TABLE OF CONTENTS

(a)

(b)

Figure S1. Detailed scheme of the RGA plasma reactor: side view (a) and cross section (b). The dimensions are presented in mm. The spark plug (serving as the ground electrode) is marked in black in the bottom image.

ST1. *Pressure and mass flow rates*

In order to confirm that the mass flow controllers provided a constant mass flow rate within the used range of pressure values, we performed tests with N_2 at four different pressures (0-3 barg), as shown in Figure S2. The gas (N_2) was supplied using an MFC into the inlet of the same reactor, and regulated and monitored in the same way as described above, and is shown in Figure S2. A mass flow meter (MFM, Sensidyne Gilibrator 3) was connected to the outlet of the RGA reactor, and the volumetric flow rate of N_2 passing through it was recorded. At the mass flow rate setting on the MFC of 4 and 8 Ln/min, the mass flow rate detected by the MFM in the whole range of 0-3 barg did not deviate from 4 and 8 Ln/min by more than 0.6% (i.e., the flow rate did not exceed 4.02 and 8.05 Ln/min,

respectively). Therefore, the mass flow rate was assumed constant due to the negligible deviations. At the same time, within the reactor an increase in pressure resulted in a lower volumetric flow rate, and hence a lower gas velocity and a longer residence time. We also note that the definition of normal liters (Ln) used in this work follows that of the MFC manufacturer, and corresponds to 0 °C, 1 atm (0 barg)[1].
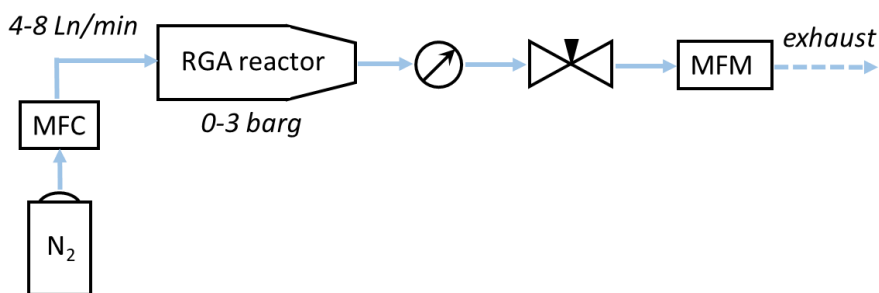
Figure S2. Schematic representation of the experiments on the MFC flow rate assessment.

ST2. *Analysis of the plasma reactor outlet for NO$_x$*

The total flow of the RGA reactor gas outlet was split using an MFC (as shown in Figure 1 in the main text), which was set to provide a post-reaction gas mixture flow of 0.5 Ln/min into the NDIR analyzer. The analyzer comprised three individual NO$_x$ sensors: NO, NO$_2$ (0-20 and 0-10 vol%, respectively), and N$_2$O (0-2000 ppm). All sensors had detection limit (4 σ) and accuracy of ≤ 0.5%FS. Prior to each set of measurements, zero and span calibrations were performed.

The quantitative analysis was performed when the concentrations of NO and NO$_2$ reached a steady-like state, i.e., did not vary by more than 0.02 vol% within a period of at least 5 min. The NDIR was calibrated using calibration gases (16.02 vol% NO in He, 7.80 vol% NO$_2$ in He, 964 ppm N$_2$O in He) purchased from Praxair. In all experiments, no N$_2$O was detected.

ST3. *Calculation of plasma power, energy consumption and production rate values*

The plasma power was calculated as an average of instantaneous plasma power values, expressed in eq. SE1:

$$P\ (W) = \frac{1}{n}\sum_{i=1}^{n} V_i \times I_i = \frac{1}{n}\sum_{i=1}^{n} V_{HV_i}\ (V) \times I_i\ (A) = \frac{1}{n}\sum_{i=1}^{n} V_{HV_i}\ (V) \times \frac{V_{shunt_i}\ (V)}{R_{shunt}\ (\Omega)} \tag{SE1}$$

The plasma power-based and the plug-to-NO_x energy consumption (EC) were calculated as shown in eq. SE2 and SE3, respectively:

$$EC\ \left(\frac{MJ}{mol}\right) = \frac{Plasma\ power\ (W)}{\frac{Mass\ flow\ rate\ _{total\ NO_x}\left(\frac{Ln}{min}\right)}{22.4\left(\frac{Ln}{mol}\right) \times 60\left(\frac{s}{min}\right)}} \times 10^{-6}\ \left(\frac{MJ}{J}\right) \tag{SE2}$$

$$Plug - to - NO_x\ EC\ \left(\frac{MJ}{mol}\right) = \frac{Power\ consumed\ by\ the\ PSU\ (W)}{\frac{Mass\ flow\ rate\ _{total\ NO_x}\left(\frac{Ln}{min}\right)}{22.4\left(\frac{Ln}{mol}\right) \times 60\left(\frac{s}{min}\right)}} \times 10^{-6}\ \left(\frac{MJ}{J}\right) \tag{SE3}$$

where the mass flow rates are calculated using eq. SE4 and SE5:

$$Mass\ flow\ rate_{total\ NO_x}\left(\frac{Ln}{min}\right) = \sum Mass\ flow\ rate_{NO_x}\left(\frac{Ln}{min}\right) \tag{SE4}$$

$$Mass\ flow\ rate_{NO_x}\left(\frac{Ln}{min}\right) = \frac{\left(Mass\ flow\ rate_{N_2}^{inlet} + Mass\ flow\ rate_{O_2}^{inlet}\right)\left(\frac{Ln}{min}\right) \times \frac{C_{NO_x}\ (ppm)}{10^6}}{1 + \frac{C_{NO_2}\ (ppm)}{2 \times 10^6}} \tag{SE5}$$

Similarly, total NO_x production rate (PR) was calculated as in eq. SE6:

$$\sum PR_{NO_x}\left(\frac{g}{h}\right) = \frac{Mass\ flow\ rate_{NO}\left(\frac{Ln}{min}\right) \times 30\left(\frac{g}{mol}\right) + Mass\ flow\ rate_{NO_2}\left(\frac{Ln}{min}\right) \times 46\left(\frac{g}{mol}\right)}{22.4\left(\frac{Ln}{mol}\right)} \times 60\left(\frac{min}{h}\right) \tag{SE6}$$

We specifically note that the formulae presented in eq. SE2-SE6 account for the gas contraction due to the stoichiometry of the NO_2 formation, which is often overlooked in literature reports. We imply that when reporting an important metric such as EC or PR, the gas contraction must be taken into account, in order to present data accurately.
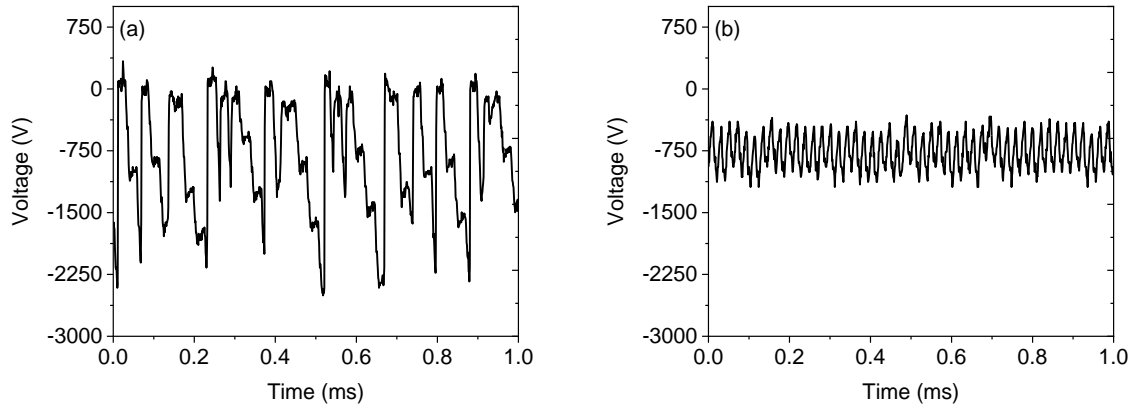
Figure S3. Voltage as a function of time for the restrike (a) and takeover mode (b).
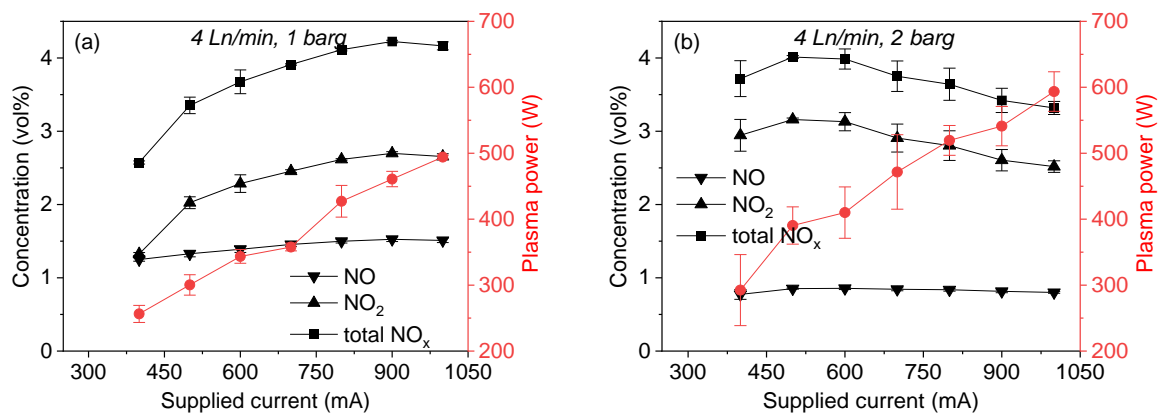
Figure S4. Concentration of produced NO_x and plasma power with N_2:O_2 4:1, at 4 Ln/min, 1 barg (a) and 2 barg (b) as a function of the current supplied by the PSU. The results are presented for conditions which produced the stable takeover discharge mode.
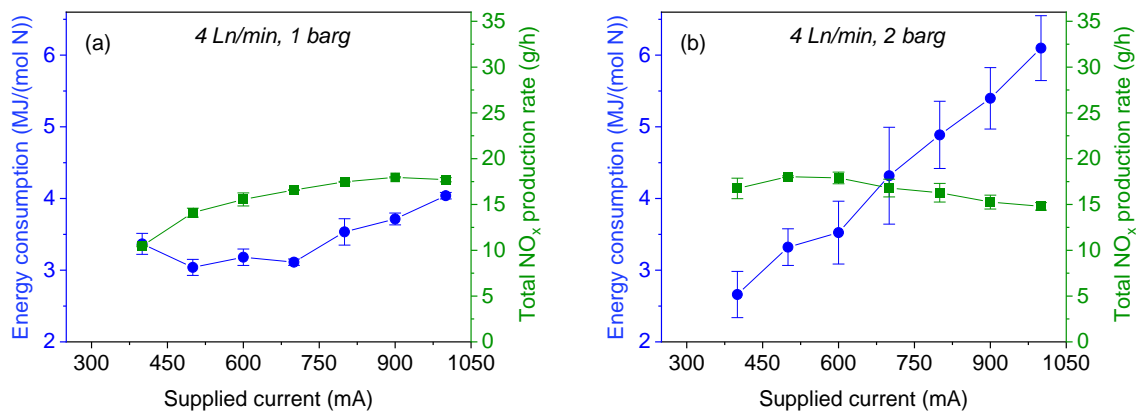
Figure S5. Energy consumption and total NO_x production rate with N_2:O_2 4:1, at 4 Ln/min, 1 barg (a) and 2 barg (b) as a function of the current supplied by the PSU. The results are presented for conditions which produced the stable takeover discharge mode.
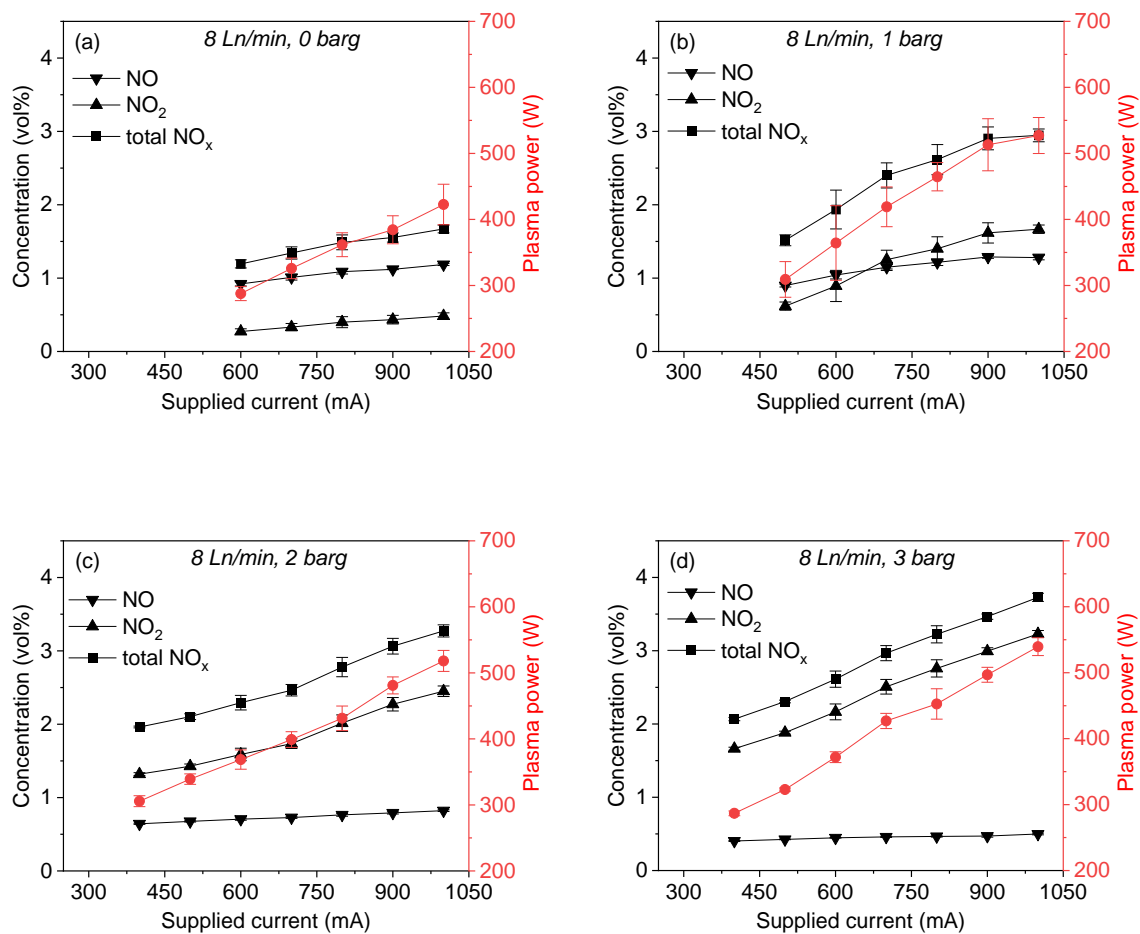
Figure S6. Concentration of the produced NO_x and plasma power with $N_2:O_2$ 4:1, at 8 Ln/min, 0 barg (a), 1 barg (b), 2 barg (c) and 3 barg (d) as a function of the current supplied by the PSU. The results are presented for conditions which produced the stable takeover discharge mode.
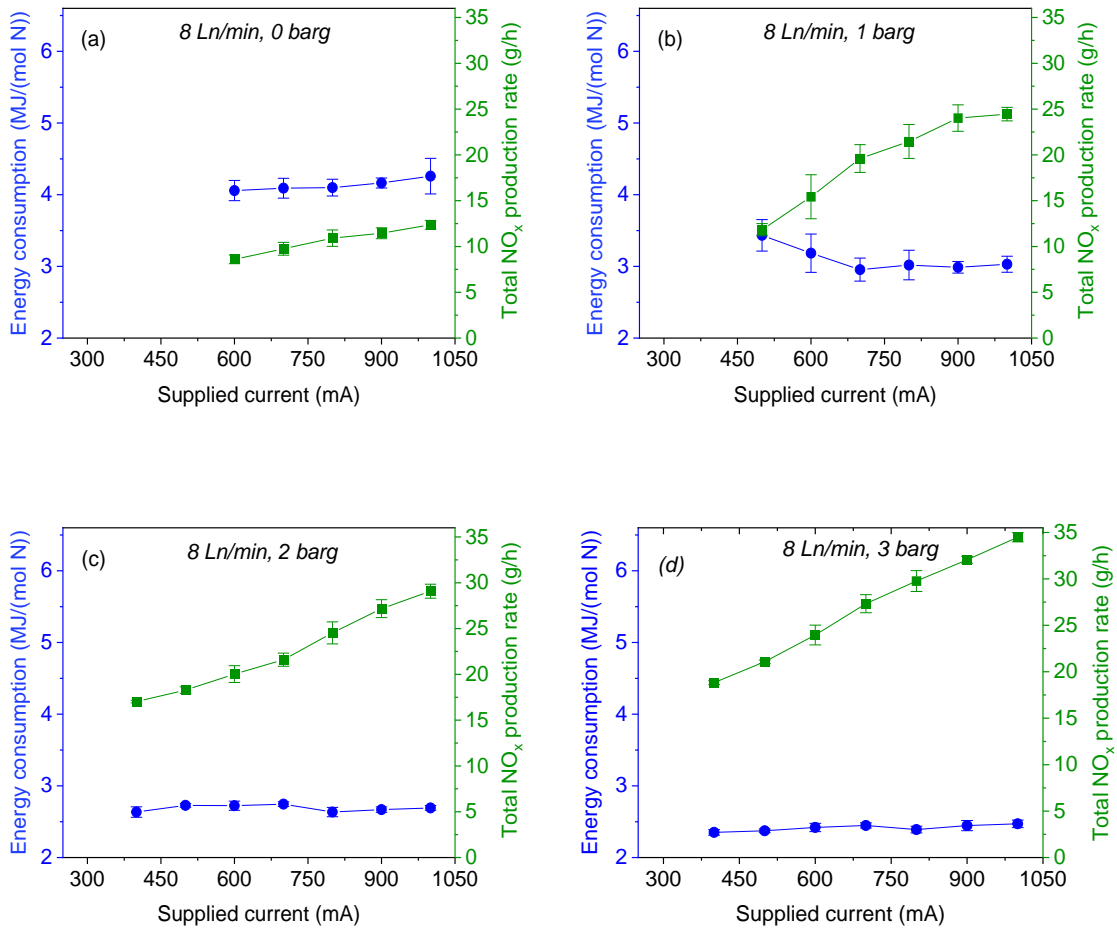
Figure S7. Energy consumption and total NO_x production rate with $N_2:O_2$ 4:1, at 8 Ln/min, 0 barg (a), 1 barg (b), 2 barg (c) and 3 barg (d) as a function of the current supplied by the PSU. The results are presented for conditions which produced the stable takeover discharge mode.
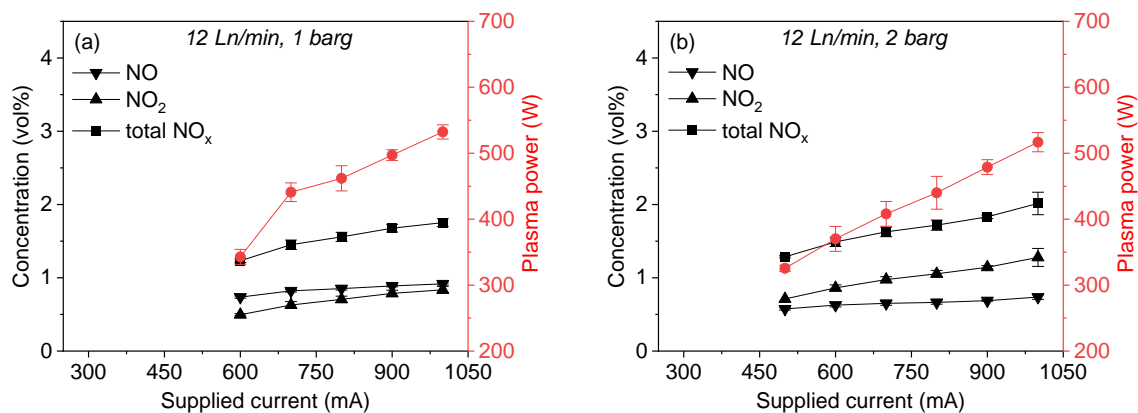
Figure S8. Concentration of produced NO_x and plasma power with N_2:O_2 4:1, at 12 Ln/min, 1 barg (a) and 2 barg (b) as a function of the current supplied by the PSU. The results are presented for conditions which produced the stable takeover discharge mode.
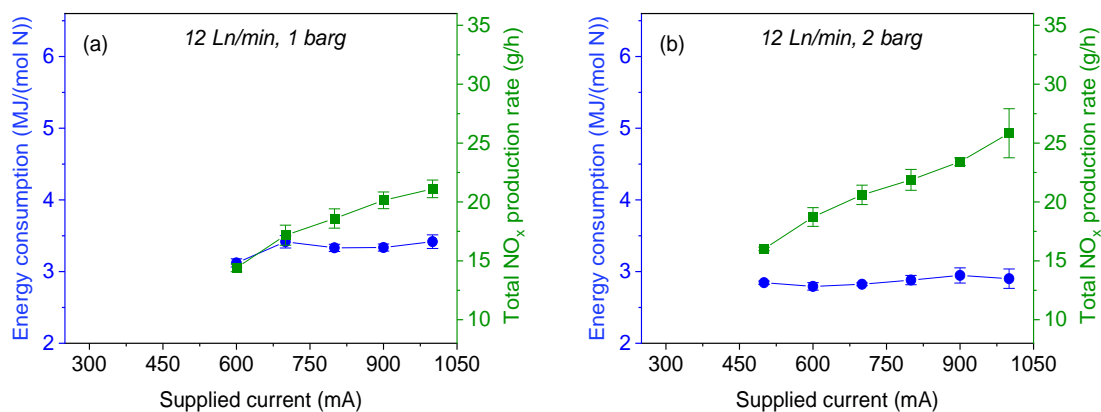
Figure S9. Energy consumption and total NO_x production rate with N_2:O_2 4:1, at 12 Ln/min, 1 barg (a) and 2 barg (b) as a function of the current supplied by the PSU. The results are presented for conditions which produced the stable takeover discharge mode.

Table S1. Comparison of production rate (PR) and plasma-based energy consumption (EC) at constant flow rate and power for different pressures and $N_2:O_2$ ratios.

Entry	Flow rate (Ln/min)	Pressure (barg)	Power (W)	PR (g/h)	EC (MJ/(mol N))
			$N_2:O_2$ feed gas ratio 4:1		
1	4	0	404	15.5	3.5
2	4	1	427	17.5	3.5
3	4	2	410	17.9	3.3
4	4	3	403	17.9	3.6
5	8	0	423	12.4	4.3
6	8	1	419	19.6	3.0
7	8	2	431	24.5	2.6
8	8	3	427	27.3	2.5
9	12	0	437	11.3	4.7
10	12	1	441	17.2	3.4
11	12	2	440	21.9	2.9
12	12	3	430	28.3	2.3
			$N_2:O_2$ feed gas ratio 1:1		
13	4	0	439	15.7	4.0
14	4	1	439	22.2	3.1
15	4	2	456	23.0	3.2
16	4	3	445	22.2	3.3
17	8	0	641	21.0	4.2
18	8	1	640	37.6	2.6
19	8	2	642	45.6	2.3
20	8	3	617	46.9	2.1
21	12	0	710	29.5	3.3
22	12	1	758	59.0	1.9
23	12	2	766	68.7	1.8
24	12	3	765	68.9	1.8

Table S2. Measured values of power consumed by the PSU, and the plug-to-NO$_x$ energy consumption (EC), for different experimental conditions with the N$_2$:O$_2$ ratio 4:1.

Pressure (barg)	Supplied current (mA)	Power consumed by PSU (W)			Plug-to-NO$_x$ EC (MJ/(mol N))		
				4 Ln/min			
0	500	786.7	±	37.7	9.5	±	0.9
	600	903.3	±	12.5	9.8	±	0.6
	700	1053.3	±	34.0	10.1	±	0.3
	800	1186.7	±	26.2	10.9	±	0.2
	900	1313.3	±	12.5	11.4	±	0.2
	1000	1440.0	±	14.1	12.0	±	0.1
1	400	660.0	±	0.0	8.7	±	0.1
	500	786.7	±	9.4	8.0	±	0.4
	600	913.3	±	9.4	8.5	±	0.3
	700	1080.0	±	63.8	9.4	±	0.6
	800	1273.3	±	4.7	10.5	±	0.1
	900	1366.7	±	17.0	11.0	±	0.2
	1000	1486.7	±	4.7	12.2	±	0.2
2	400	686.7	±	9.4	6.3	±	0.4
	500	803.3	±	17.0	6.8	±	0.1
	600	950.0	±	8.2	8.1	±	0.3
	700	1063.3	±	4.7	9.7	±	0.5
	800	1280.0	±	16.3	12.0	±	0.7
	900	1380.0	±	0.0	13.9	±	0.6
	1000	1513.3	±	4.7	15.5	±	0.4
3	300	583.3	±	4.7	6.2	±	0.7
	400	696.7	±	4.7	6.0	±	0.1
	500	820.0	±	8.2	7.3	±	0.2
	600	960.0	±	8.2	8.8	±	0.5
	700	1070.0	±	8.2	10.7	±	0.1
	800	1290.0	±	14.1	13.2	±	0.3
	900	1393.3	±	9.4	14.5	±	0.1
	1000	1530.0	±	0.0	16.5	±	0.1
				8 Ln/min			
0	600	966.7	±	59.1	14.0	±	1.3

	700	1123.3	±	30.9	14.6	±	0.8
	800	1283.3	±	12.5	15.0	±	0.7
	900	1413.3	±	17.0	15.7	±	0.2
	1000	1520.0	±	8.2	15.6	±	0.3
	500	830.0	±	8.2	9.2	±	0.4
	600	976.7	±	9.4	8.7	±	1.4
1	700	1110.0	±	8.2	7.9	±	0.6
	800	1256.7	±	9.4	8.2	±	0.6
	900	1410.0	±	0.0	8.2	±	0.5
	1000	1570.0	±	0.0	9.0	±	0.3
	400	713.3	±	12.5	6.2	±	0.1
	500	840.0	±	8.2	6.8	±	0.1
	600	980.0	±	16.3	7.3	±	0.4
2	700	1143.3	±	9.4	7.9	±	0.3
	800	1300.0	±	0.0	8.0	±	0.4
	900	1436.7	±	9.4	8.0	±	0.3
	1000	1593.3	±	9.4	8.3	±	0.3
	400	723.3	±	9.4	5.9	±	0.1
	500	866.7	±	17.0	6.4	±	0.1
	600	996.7	±	9.4	6.5	±	0.3
3	700	1170.0	±	21.6	6.7	±	0.4
	800	1306.7	±	4.7	6.9	±	0.3
	900	1446.7	±	9.4	7.1	±	0.1
	1000	1616.7	±	12.5	7.4	±	0.1

12 Ln/min

	600	1013.3	±	17.0	12.9	±	0.3
	700	1130.0	±	14.1	12.2	±	0.6
0	800	1293.3	±	40.3	12.0	±	0.5
	900	1430.0	±	28.3	12.1	±	0.3
	1000	1570.0	±	8.2	13.0	±	0.2
	600	1000.0	±	8.2	9.1	±	0.1
	700	1146.7	±	12.5	8.9	±	0.5
1	800	1300.0	±	8.2	9.4	±	0.4
	900	1446.7	±	12.5	9.7	±	0.4
	1000	1610.0	±	8.2	10.3	±	0.3
2	500	856.7	±	9.4	7.5	±	0.1
	600	1006.7	±	17.0	7.6	±	0.2

	700	1163.3	±	12.5		8.1	±	0.2
	800	1320.0	±	8.2		8.7	±	0.3
	900	1476.7	±	12.5		9.1	±	0.2
	1000	1640.0	±	8.2		9.2	±	0.7
	400	726.7	±	30.9		5.4	±	0.3
	500	883.3	±	26.2		5.7	±	0.3
	600	1000.0	±	0.0		5.9	±	0.3
3	700	1180.0	±	32.7		6.4	±	0.3
	800	1340.0	±	14.1		6.8	±	0.3
	900	1466.7	±	12.5		7.0	±	0.4
	1000	1640.0	±	0.0		7.5	±	0.5

ST4. *Calculation of equilibrium NO concentration.*

The calculation for the equilibrium NO concentration is performed using the sigmoidal fitting functions provided by D'Angola et al.[2] :

$$\sigma(T, c, \Delta) = \frac{e^q}{e^q + e^{-q}}, \qquad q = \frac{T - c}{\Delta} \tag{SE7}$$

where T is the gas temperature. The dependence of the sigmoid on pressure is expressed through the fitting constants c and Δ.

$$\sigma_i(T, c, \Delta) = \sigma(T, c_i, \Delta_i) \tag{SE8}$$

The pressure-dependent parameters c, Δ, a are expressed as a function of the pressure logarithm as:

$$logC = \sum_{j=0}^{n} \alpha_j x^j \tag{SE9}$$

Where $logC$ represents any of the fitting parameters and $x = \log(P)$ is the logarithm of the pressure P.

The concentration of NO is given as:

$$NO\ vol\% = 100 \times \max\left[0, \sum_{j=1}^{n} a_j \sigma_j(T)\right]$$ (SE10)

The values of the fitting constants are listed in Table S3.

Table S3. Constants for determining the pressure-dependent concentration of NO.

		α_0	α_1	α_2	α_3	α_4
σ_1	$\log a_1$	-2.397641	9.644207e-2	-	-	-
	$\log c_1$	7.942600	2.917164e-2	6.775381e-4	2.209082e-5	-
	$\log \Delta_1$	6.780323	6.029139e-2	4.276063e-4	-	-
σ_2	$a_2 = -a_1 - a_3$	-	-	-	-	-
	$\log c_2$	8.274503	6.655621e-2	2.214534e-3	3.856329e-5	
	$\log \Delta_2$	6.495225	7.930874e-2	−1.952605e-3	−7.384374e-4	−5.231985e-5
σ_3	$\log(-a_3)$	−2.923272	1.671984e-1	-	-	-
	$\log c_3$	8.364477	7.365241e-2	2.771836e-3	−5.013391e-6	−5.293616e-6
	$\log \Delta_3$	7.549495	9.399569e-2			

ST5. *Calculation of the pressure-dependent rate coefficient R5.*

The pressure-dependent rate coefficient is calculated by adding a broadening factor F to the Lindemann-Hinshelwood relation as described in Baulch et al. [3]:

$$k = k_\infty \left(\frac{k_0[M]/k_\infty}{1 + k_0[M]/k_\infty} \right) F \tag{SE11}$$

Where k is the reaction rate coefficient, $k_\infty = 4.9 \cdot 10^{-10} T^{-0.4} \frac{cm^3}{s}$ is the reaction rate coefficient in the high-pressure limit, $k_0 = 9.2 \cdot 10^{-28} T^{-1.6} \frac{cm^6}{s}$ is the reaction rate coefficient in the low pressure limit, and $[M]$ is the gas number density calculated from the ideal gas law.

The broadening factor F is given by:

$$\log F = \frac{\log F_c}{1 + \left[\frac{\log \left(\frac{k_0[M]}{k_\infty} \right)}{N} \right]^2} \tag{SE12}$$

Where $N = 0.75 - 1.27 \log F_c$ and $F_c = 0.8$.
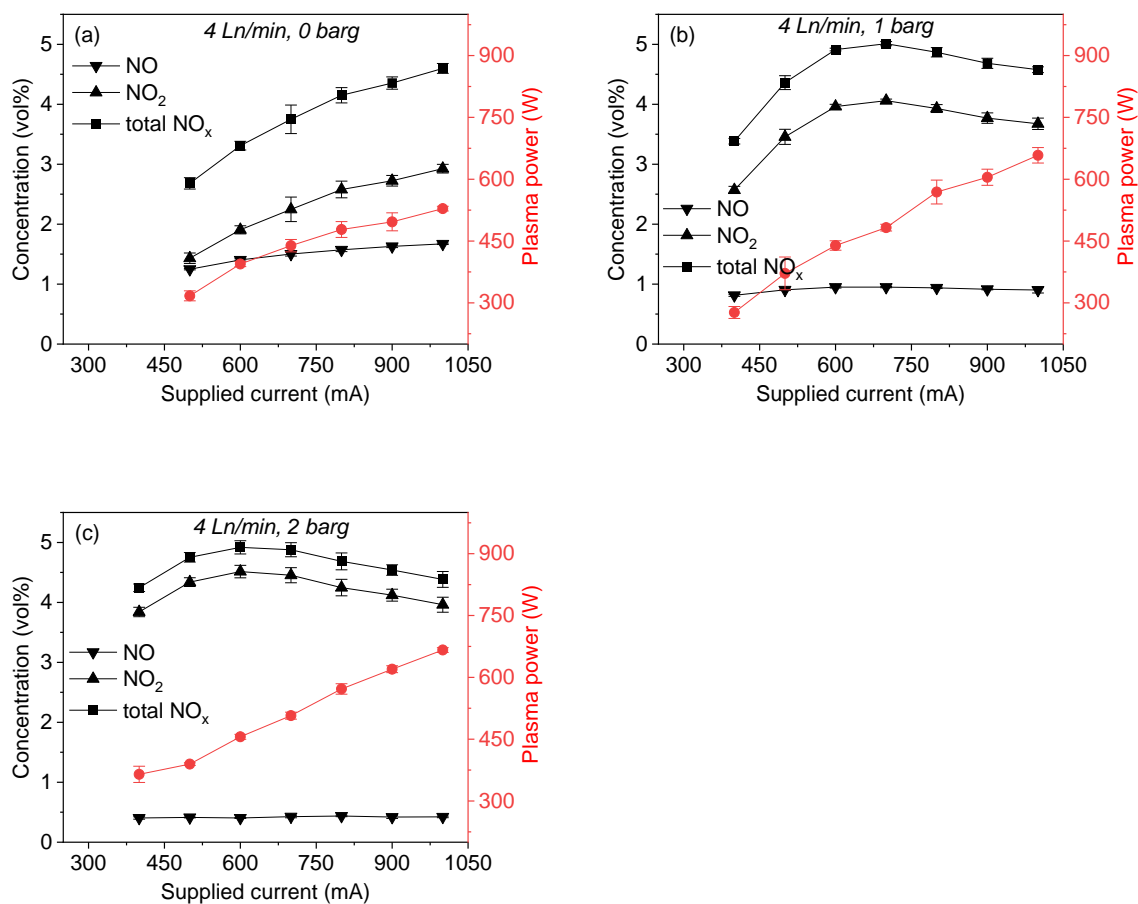
Figure S10. Concentration of produced NO_x and plasma power with N_2:O_2 1:1, at 4 Ln/min, 0 barg (a), 1 barg (b), and 2 barg (c) as a function of the current supplied by the PSU. The results are presented for conditions which produced the stable takeover discharge mode.
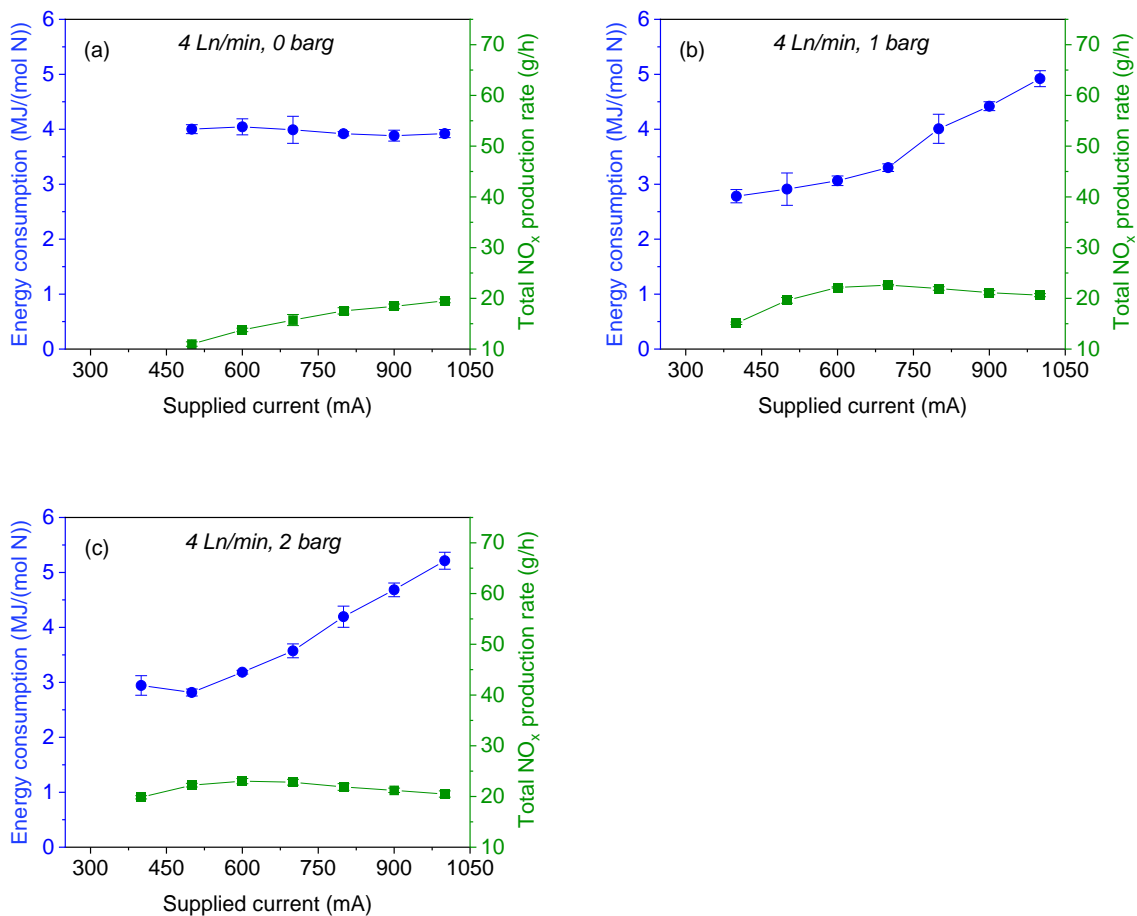
Figure S11. Energy consumption and total NO_x production rate with $N_2:O_2$ 1:1, at 4 Ln/min, 0 barg (a), 1 barg (b), and 2 barg (c) as a function of the current supplied by the PSU. The results are presented for conditions which produced the stable takeover discharge mode.
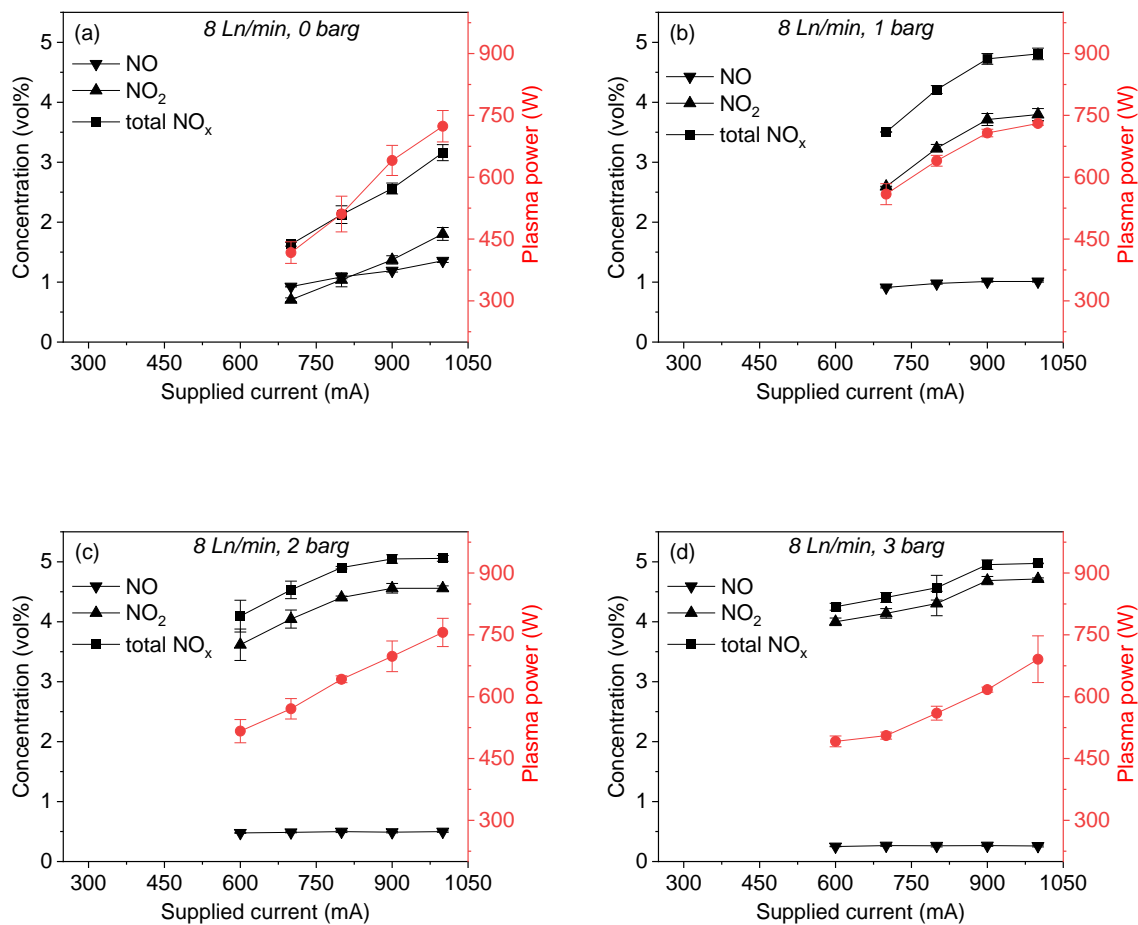
Figure S12. Concentration of produced NO_x and plasma power with $N_2:O_2$ 1:1, at 8 Ln/min, 0 barg (a), 1 barg (b), 2 barg (c), and 3 barg (d) as a function of the current supplied by the PSU. The results are presented for conditions which produced the stable takeover discharge mode.
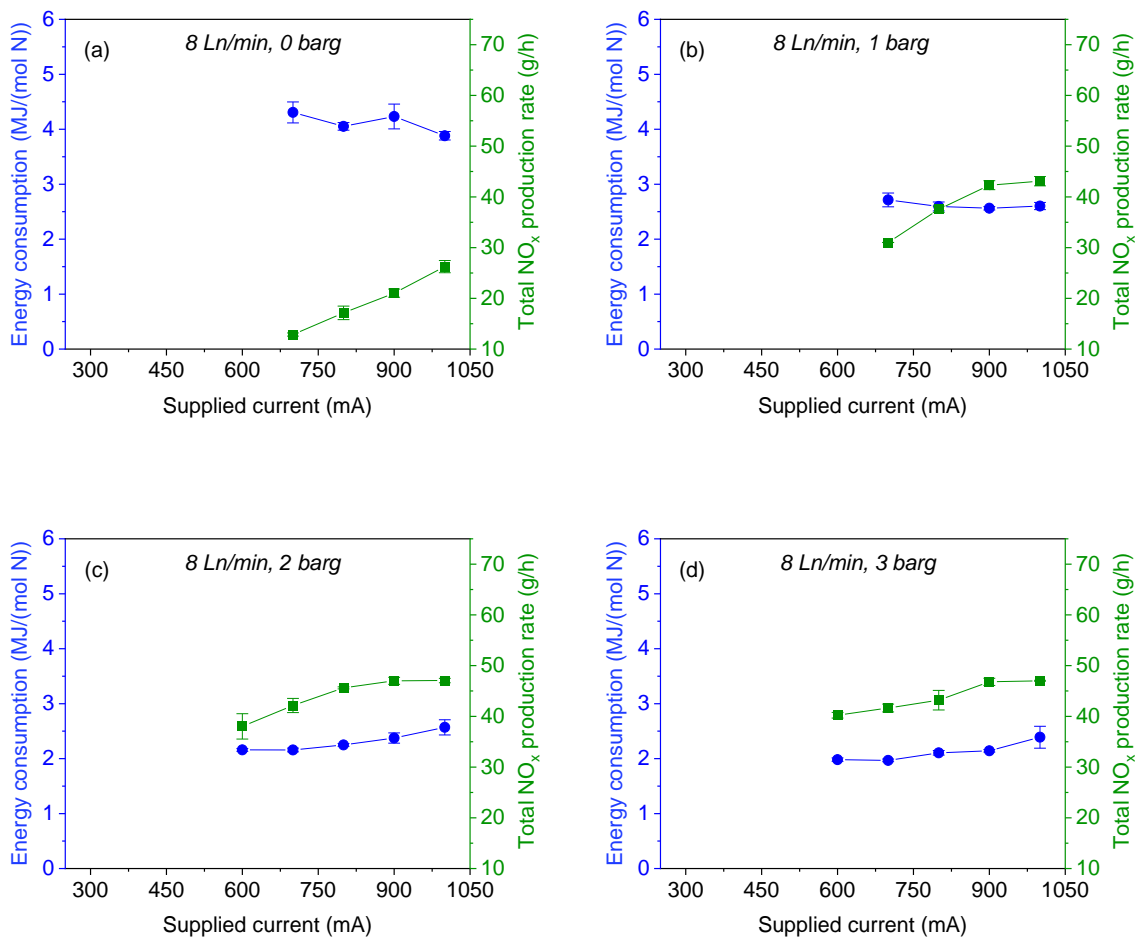
Figure S13. Energy consumption and total NO_x production rate with N_2:O_2 1:1, at 8 Ln/min, 0 barg (a), 1 barg (b), 2 barg (c), and 3 barg (d) as a function of the current supplied by the PSU. The results are presented for conditions which produced the stable takeover discharge mode.
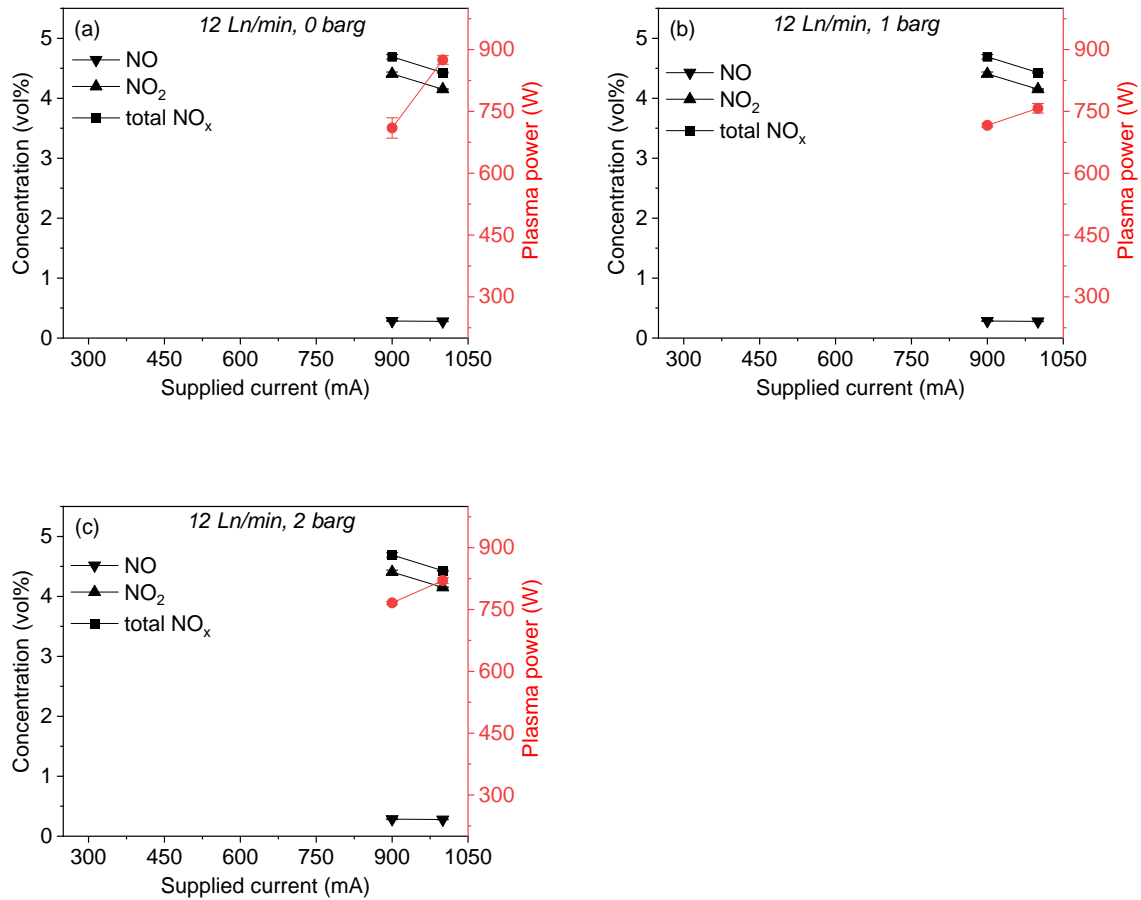
Figure S14. Concentration of produced NO_x and plasma power with $N_2:O_2$ 1:1, at 12 Ln/min, 0 barg (a), 1 barg (b), and 2 barg (c) as a function of the current supplied by the PSU. The results are presented for conditions which produced the stable takeover discharge mode.
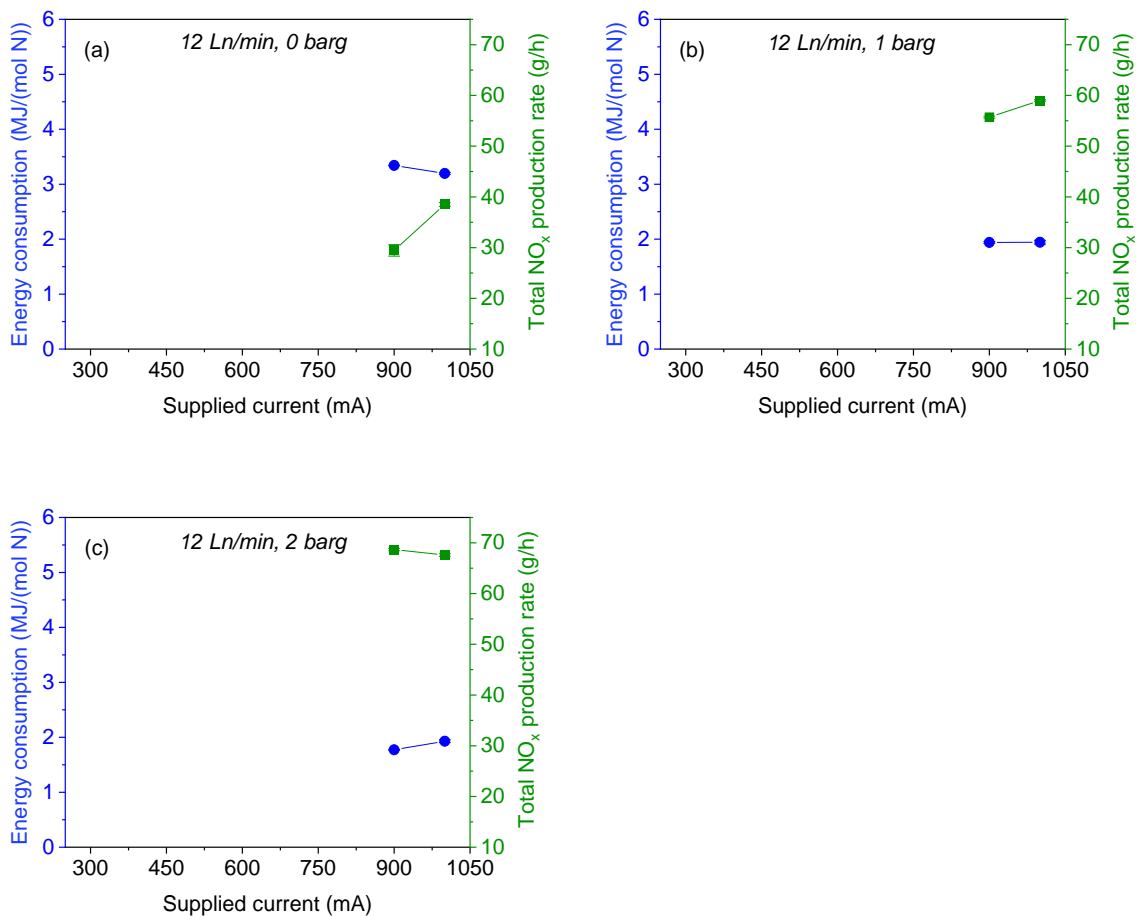
Figure S15. Energy consumption and total NO_x production rate with $N_2:O_2$ 1:1, at 12 Ln/min, 0 barg (a), 1 barg (b) and 2 barg (c) as a function of the current supplied by the PSU. The results are presented for conditions which produced the stable takeover discharge mode.

Table S4. Measured values of power consumed by the PSU, and the plug-to-NO$_x$ energy consumption (EC), for different experimental conditions with the N$_2$:O$_2$ ratio 1:1.

Pressure (barg)	Supplied current (mA)	Power consumed by PSU (W)	Plug-to-NO$_x$ EC (MJ/(mol N))
		4 Ln/min	
0	500	713.3 ± 9.4	9.0 ± 0.4
	600	856.7 ± 17.0	8.8 ± 0.4
	700	1003.3 ± 26.2	9.1 ± 0.7
	800	1150.0 ± 35.6	9.4 ± 0.4
	900	1276.7 ± 23.6	10.0 ± 0.1
	1000	1410.0 ± 8.2	10.5 ± 0.1
1	400	576.7 ± 20.5	5.8 ± 0.2
	500	736.7 ± 24.9	5.8 ± 0.2
	600	853.3 ± 30.9	6.0 ± 0.2
	700	1016.7 ± 18.9	7.0 ± 0.1
	800	1183.3 ± 33.0	8.3 ± 0.4
	900	1333.3 ± 9.4	9.8 ± 0.2
	1000	1500.0 ± 8.2	11.2 ± 0.1
2	400	603.3 ± 4.7	4.9 ± 0.1
	500	746.7 ± 12.5	5.4 ± 0.1
	600	886.7 ± 4.7	6.2 ± 0.2
	700	1010.0 ± 16.3	7.1 ± 0.2
	800	1176.7 ± 12.5	8.6 ± 0.2
	900	1336.7 ± 17.0	10.1 ± 0.3
	1000	1500.0 ± 16.3	11.7 ± 0.4
3	400	663.3 ± 30.9	4.9 ± 0.2
	500	786.7 ± 26.2	5.8 ± 0.3
	600	930.0 ± 37.4	7.3 ± 0.7
	700	1073.3 ± 33.0	8.6 ± 0.8
	800	1196.7 ± 4.7	10.0 ± 0.4
	900	1360.0 ± 14.1	11.5 ± 0.2
	1000	1500.0 ± 14.1	12.7 ± 0.3
		8 Ln/min	
0	700	1083.3 ± 83.8	11.2 ± 0.7
	800	1253.3 ± 75.9	10.0 ± 0.1

	900	1446.7	±	12.5	9.6	±	0.3
	1000	1543.3	±	33.0	8.3	±	0.5
1	700	1110.0	±	32.7	5.4	±	0.2
	800	1286.7	±	9.4	5.2	±	0.1
	900	1460.0	±	8.2	5.3	±	0.1
	1000	1580.0	±	0.0	5.6	±	0.1
2	600	916.7	±	54.4	3.8	±	0.1
	700	1110.0	±	21.6	4.2	±	0.1
	800	1280.0	±	16.3	4.5	±	0.1
	900	1436.7	±	30.9	4.9	±	0.1
	1000	1586.7	±	9.4	5.4	±	0.1
3	600	946.7	±	20.5	3.8	±	0.1
	700	1056.7	±	20.5	4.1	±	0.1
	800	1190.0	±	29.4	4.5	±	0.1
	900	1380.0	±	16.3	4.8	±	0.1
	1000	1573.3	±	45.0	5.4	±	0.2

12 Ln/min

0	900	1543.3	±	12.5	7.3	±	0.3
	1000	1726.7	±	17.0	6.3	±	0.1
1	900	1636.7	±	18.9	4.4	±	0.1
	1000	1816.7	±	12.5	4.7	±	0.1
2	900	1720.0	±	8.2	4.0	±	0.1
	1000	1893.3	±	12.5	4.5	±	0.1
3	800	1580.0	±	8.2	3.7	±	0.1
	900	1773.3	±	4.7	4.3	±	0.1
	1000	1940.0	±	14.1	5.0	±	0.1

REFERENCES

(1) Available online at: https://www.bronkhorst.com/int/service-support-1/faq/flow-theory/what-does-bronkhorst-mean-by-ln-min-or-ls-min/ (accessed on 24.10.2022).

(2) D'Angola, A.; Colonna, G.; Gorse, C.; Capitelli, M. Thermodynamic and transport properties in equilibrium air plasmas in a wide pressure and temperature range. *Eur. Phys. J. D* **2008**, *l46*, 129–150. DOI: 10.1140/epjd/e2007-00305-4.

(3) Baulch, D. L.; Bowman, C. T.; Cobos, C. J.; Cox, R. A.; Just, T.; Kerr, J. A.; Pilling, M. J.; Stocker, D.; Troe, J.; Tsang, W.; Walker, R. W.; Warnatz, J. Evaluated Kinetic Data for Combustion Modeling: Supplement II. *J. Phys. Chem. Ref. Data* **2005**, *34*, 757-1397. DOI: 10.1063/1.1748524.